○ Heritage Science

RESEARCH ARTICLE

Polychrome arhat figures dated from the Song Dynasty (960–1279 CE) at the Lingyan Temple, Changqing, Shandong, China

Yongdong Tong[1], Youzhen Cai[2], Xuening Wang[2], Zhimin Li[3], Austin Nevin[4*] and Qinglin Ma[3*]

Abstract

Scientific analysis revealed the materials and techniques used in the process of making polychrome sculptures providing a solid foundation for the protection and restoration of the painted statues. In addition, the analyses revealed changes in colour schemes applied to the sculptures can provide the basis for the virtual restoration of the painted statues. In order to carry out scientifically-informed protection and restoration of the Bodhidharma statue from the Lingyan Temple, Changqinq, Shandong, several analytical methods such as optical microscope (OM), Micro-Raman spectroscopy (μ-RS), scanning electron microscopy coupled with energy dispersive X-ray analysis (SEM–EDS) and Fourier transform infrared spectroscopy (FTIR) were employed. Analyses clearly reveal the information including the stratigraphic structure and the composition of pigment. The use of silver foils and golden yellow pyrophyllite mineral to replace gold foils were found in the gilding paint layer in the later repainting after the Song Dynasty. This work reports the coexistence of emerald green ($Cu(C_2H_3O_2)_2 \cdot 3Cu(AsO_2)_2$) and the degradation product lavendulan ($NaCaCu_5(AsO_4)_4Cl \cdot 5H_2O$) in large areas of the paint stratigraphy and on the surface confirming that the degradation of emerald green is related to the thickness of the paint layer; in thinner paint layers emerald green is transformed in lavendulan, while thicker layers of contain both lavendulan and emerald green, suggesting an environmental source of chlorides.

Keywords: Lingyan Temple, Arhat statues, Paint layers, Scientific analysis

Introduction and the aims of research

The Lingyan Temple (灵岩寺) is located in the Lingyan mountain in Wande town (万德镇), Changqing district (长清区), Jinan, Shandong province, China, about 20 km from Mount Tai (Fig. 1). The temple is an important part of Mount Tai world natural and cultural heritage. As early as the Yuan-he period (806–820 CE) of the Tang D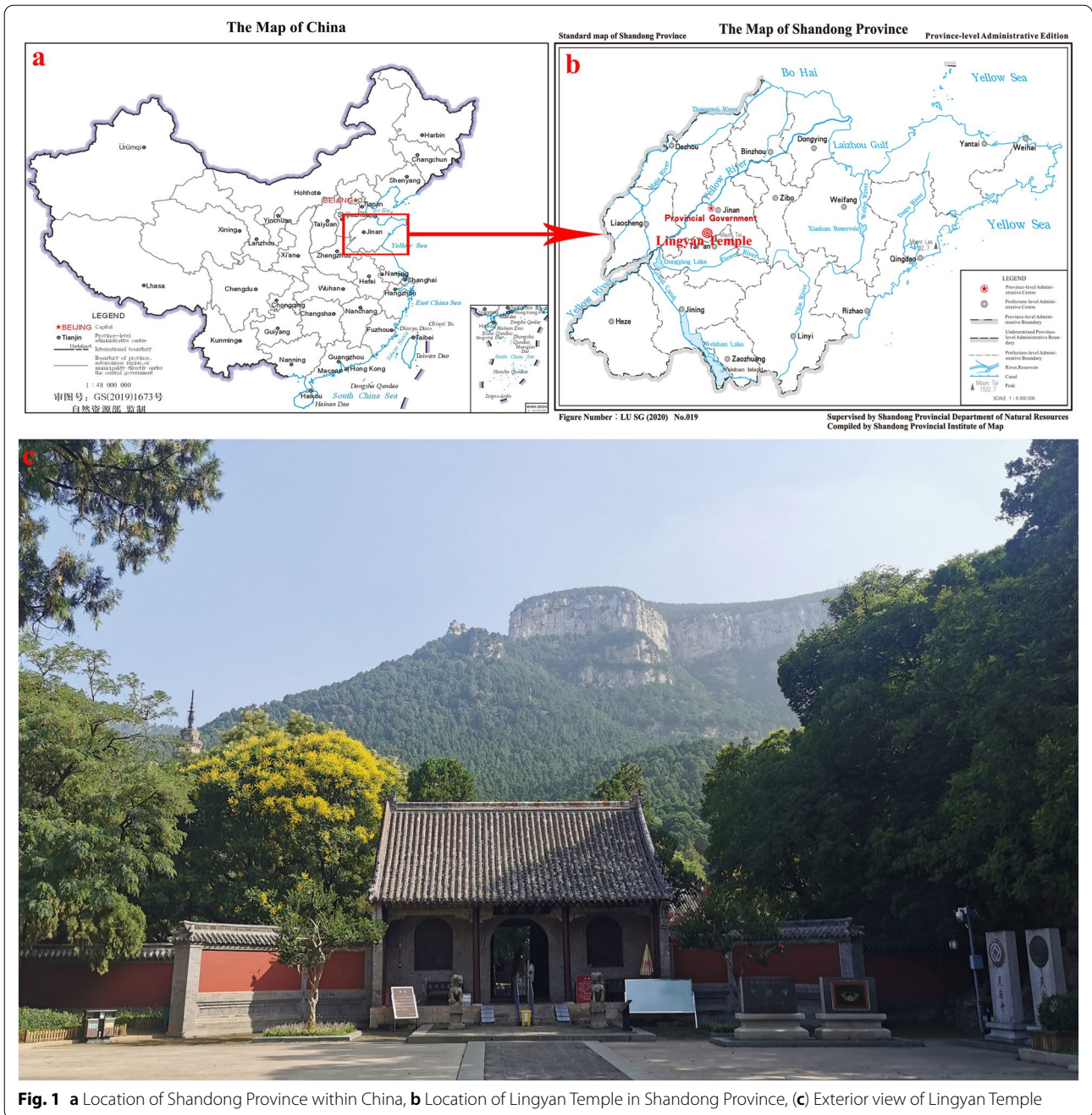ynasty (618–907 CE), Li jifu (李吉甫), a knowledgeable prime minister, reports Lingyan Temple together with Qixia Temple (栖霞寺) in Jiangsu, Guoqing Temple (国清寺) in Zhejiang and Yuquan Temple (玉泉寺) in Hubei as the "Four famous temples in Chinese domain". The extant stele inscriptions record that the Lingyan Temple ranked first among the four famous temples in the Song Dynasty. After the founding of the People's Republic of China, Lingyan Temple was classified in 1982 as a national key cultural relic. There are many precious historical relics in Lingyan Temple, such as Pizhi pagoda (辟支塔), the forest of stupas (墓塔林), stone inscriptions (there are more than 700 pieces) and many ancient buildings and ruins. Among the numerous precious historical relics, 40 painted arhat statues dating from the Song and Ming

*Correspondence: austinnevin@gmail.com; qinglinma226@126.com
[3] International Joint Research Laboratory of Environmental and Social Archaeology, Shandong University, Qingdao 266237, Shandong, China
[4] Courtauld Institute of Art, Somerset House, Strand, London WC2R 0RN, UK
Full list of author information is available at the end of the article

Tong *et al. Herit Sci* (2021) 9:117

Page 2 of 21

Fig. 1 **a** Location of Shandong Province within China, **b** Location of Lingyan Temple in Shandong Province, (**c**) Exterior view of Lingyan Temple

(1368–1644 CE) Dynasties are preserved in the Qianfo hall (千佛殿). These polychrome statues, especially the works of Song Dynasty, are skilfully sculpted with vivid and lifelike characters, and are recognized as rare masterpieces among ancient Chinese sculptures, and were once praised as the first famous statues in China by Mr. Liang Qichao (梁启超).

In May 1981, Jinan cultural relics management committee, Jinan museum and the Lingyan Temple cultural relics management institute of Changqing county jointly initiated the protection and repair of the arhat statues of Lingyan Temple [1]. In the process of maintenance, C-14 dating of the wooden structures within some of the arhat sculptures determined that of the 40 arhat statues, 27 were from the Song Dynasty and 13 date to the Ming Dynasty [1, 2]. The objective of this paper is the Bodhidharma (菩提达摩) statue, which is a typical Song Dynasty work. This statue is colorful

Tong *et al. Herit Sci*   (2021) 9:117

Page 3 of 21

and rich, the expression of the characters is solemn and serene, tolerant and introspective. The statue is also well preserved and has extremely high artistic value. Bodhidharma was a native of India who came to China during the Northern and Southern Dynasties (420–589 CE) and founded Chinese Zen Buddhism (禅宗). Because of the spread and popularity of Zen Buddhism in China, Bodhidharma was a household name in China. The statue of Bodhidharma was placed at the first place on the right hand side of the entrance to the Qianfo Hall, which meant the statue received more attention and favor from visitors than other statues.

For a long time, natural aging and many environmental factors (such as dust, smoke, roof leakage, the presence of insects, pollution.) lead to degradation of pigments, efflorescence and the flaking and peeling of paint. It is of great significance to analyse and study the paint layers of arhat statues for the subsequent conservation and virtual restoration. In 2018, Wang Chuanchang and others analysed samples from the sixth and seventeenth arhat statues in the east of the Qianfo Hall, and determined the mineral composition of various mineral pigments [3]. Besides that, there was little scientific analysis and research on the paint layers of arhat statues of Lingyan Temple. Complementary and multiple analytical techniques are widely used in the study of paint layers of painted cultural relics such as polychrome statues [4–7], mural paintings [8–11], painted pottery [12, 13] and so on, which can successfully reveal the microscopic structure of paint layers, the composition of the pigment and the priming layers, the types of binding media found in paint layers, repair materials, and the paint stratigraphy. In this paper, multiple analytical techniques including ultra depth of field 3D microscopy (OM), Micro-Raman spectroscopy (μ-RS), scanning electron microscopy coupled with energy dispersive X-ray analysis (SEM–EDS) and Fourier transform infrared spectroscopy (FTIR), etc. were applied to analyse the paint layers from the Bodhidharma statue. The purpose of this study is to reveal the materials and techniques used in the making the painted statues, and the changes to the composition of the paint layers as a consequence of aging, provide basic data for the protection and restoration of the painted statue and the virtual restoration of the colour texture.

Materials and methods
Materials
A total of 19 samples were collected from different colored paint on the Bodhidharma statue. The schematic diagram of sampling position was shown in Fig. 2. Except for D1–3, D1–10, D1–19, other samples were embedded in the epoxy resin and polished.

Methods
Optical microscopy (OM)
A KEYENCE VHX-6000 ultra depth of field 3D video microscope was used to observe and document the cross-sections, at magnifications from 20 to 2000×. The Leica DM2700 polarizing microscope was used for the polarizing microscopic analysis of individual pigments.

Scanning electron microscopy coupled with energy dispersive X-ray analysis (SEM–EDS)
A Tescan vega3 XMU scanning electron microscope equipped with a Bruker XFlash 610 M X-ray energy spectrometer was used to analyse the microstructural characteristics of paint layers and semi-quantitatively analyse the relative contents of major elements in pigment minerals in different layers. Analyses were carried out in a high vacuum environment, with a scanning voltage of 20 kv, 90 s of acquisition time at a 15 mm working distance.

Micro-Raman spectroscopy (μ-RS)
A HORIBA XploRAPLUS Raman spectrometer configured with an Olympus microscope and an integrated motorized stage were used to qualitatively analyse the mineral composition of different layers under 50× and 100× objective lenses. The blue and green pigments were analysed using a 532 nm laser, and the other pigment were analysed using the 785 nm laser. The laser output power ranged of 15–30 mW (532 nm) and 10–50 mW (785 nm), the spectral range of 50–2000 cm^{-1}, and the collection time was 15–25 s with 2 acculumations. The instrument was calibrated using the 520 cm^{-1} silicon Raman band.

Fourier transform infrared microscopy (FTIR)
A Thermo Nicolet iN10 MX Fourier transform infrared spectrometer was used to study the priming materials of paint layers based on the preparation of dispersions in KBr in the spectral range of 4000–400 cm^{-1}, at spectral resolution of 4 cm^{-1}.

Spectrophotometer
A X-Rite VS450 non-contact desktop spectrophotometer was used to measure the L*a*b* values of different colours at each sampling position on the statue surface. Measuring aperture 6 mm, measuring distance 1.5 inch.

Tong *et al. Herit Sci* (2021) 9:117

Page 4 of 21

Fig. 2 The statue of Bodhidharma, Lingyan Temple. Location of sampling positions

Results and discussion

The EDS results of relative elemental composition in each layer of the painting and the attribution from μ-RS analyses are shown in Table 2. The elemental composition is given as the mass percentage after normalization treatment. In the processing of element relative content analysis, the free selection mode was used to select areas of interest within each layer. The layers sequence was numbered in the micrographs of cross-sections in Fig. 3, 4 and 8 correspond to the same numbers used in EDS analysis. The M lines were chosen to quantify the Pb. Organic layers that did not contain metal ions are: D1−2 L0; D1−9 L2, L5, L8, L10, L12, L14; and D1−16 L1, L3, etc. The elemental composition of these layers are not listed in Table 2.

Analysis of stratigraphy

The cross-sections observed under the optical and scanning electron microscope clearly show that the paint layers contains multiple layers of pigments and priming layers. D1−1, D1−7and D1−9 are samples with the most layers. As shown in Fig. 3a and b, D1−1 has 14 layers from the statue surface to the unpainted clay ground, among which are seven pigment layers, and the layers structure distribution are as follows: L1 reddish-brown pigment layer → L2 white priming layer → L3 red pigment layer → L4 white priming layer → L5 orange pigment layer → L6 white priming layer → L7 yellow pigment layer → L8 white priming layer (mixed with red pigment particles) → L9 orange pigment layer → L10 white priming layer → L11 red pigment layer → L12 white priming layer → L13 white pigment layer → L14 gray priming layer.

Tong *et al. Herit Sci*   (2021) 9:117
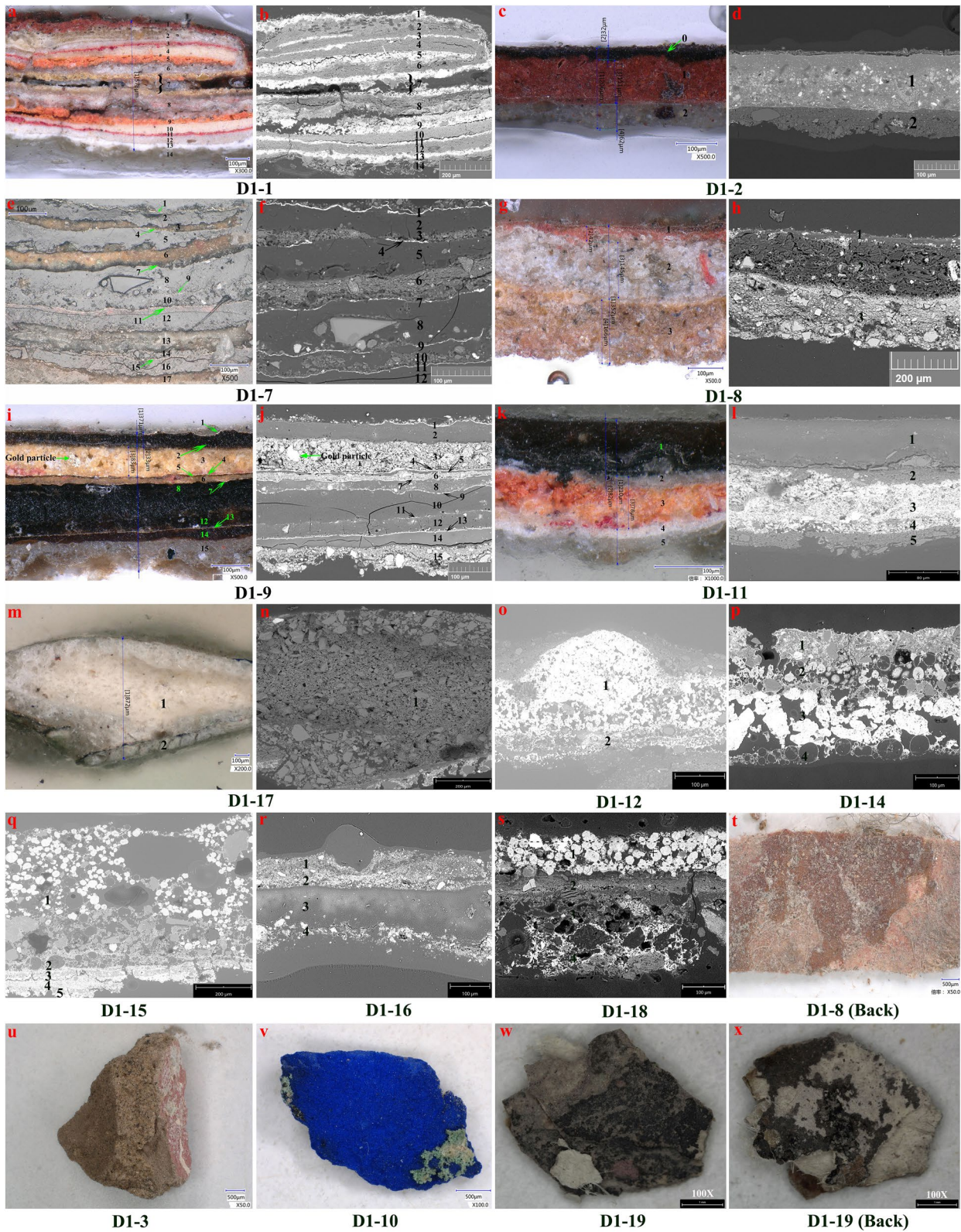
Page 5 of 21
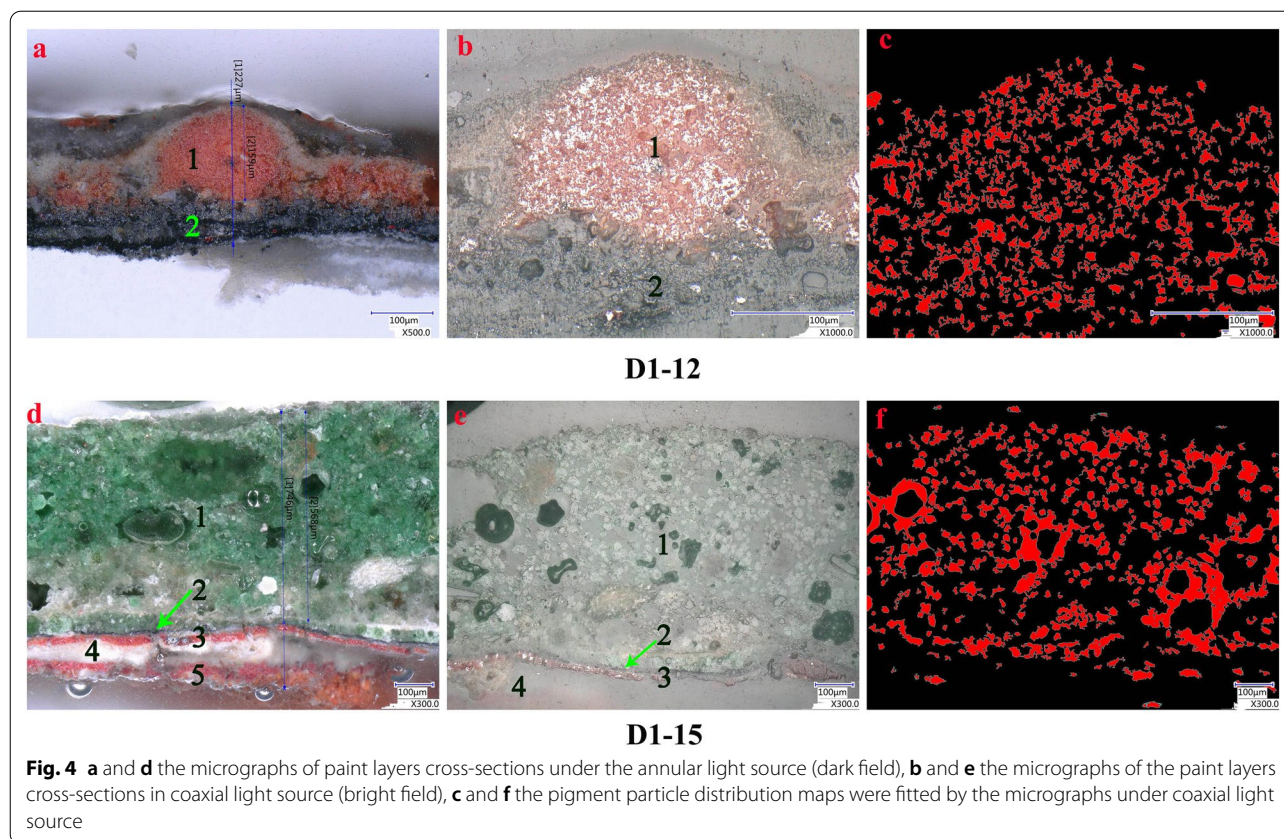

Fig. 3 **a–n** the OM micrographs and BSE images of samples cross-section revealing paint stratigraphy, **o**–**s** the BSE images of samples, **t** and **x** the micrographs of the back of samples, **u**, **v** and **w** the micrographs of samples. The numerals in the cross-section figure are in order of different layers starting from the surface of statue to the unpainted clay idol

Tong *et al. Herit Sci*   (2021) 9:117

Page 6 of 21

Fig. 4 **a** and **d** the micrographs of paint layers cross-sections under the annular light source (dark field), **b** and **e** the micrographs of the paint layers cross-sections in coaxial light source (bright field), **c** and **f** the pigment particle distribution maps were fitted by the micrographs under coaxial light source

The structural relationship between the layers of D1−9 gilding sample can be shown more clearly from the backscattered electron image (Fig. 3j). The sample from the statue surface to the unpainted clay idol totals 15 layers, including six gilding layers (L1, L4, L7, L9, L11, L13), six adhesive layers (L2, L5, L8, L10, L12, L14), two pigment layers (L3, L6), and one priming layer (L15). The layer structure of D1−7 gilding paint layer is not very clear under the optical microscope annular light source (dark field), but clearly visible under the coaxial light source (bright field) and in the backscattered electron image (as shown in Fig. 3e and f). The layer structure is basically the same as the layer structure of D1−9, but there is an extra priming layer under the 12th layer of adhesive. According to our analyses, the D1−7 and D1−9 contain six gilding layers and two pigment layers demonstrating that the Bodhidharma statue has experienced at least 8 repainting treatments.

In other samples of paint there are only two layers. As seen from Fig. 3c and d, sample D1−2 located on the face of the statue has only one reddish-brown pigment layer and one priming layer, suggesting that the color of the face has always remained the same in the previous repainting process. The reddish-brown pigment layer was covered with a dark translucent organic material (this translucent material is almost invisible in backscattered electron images).

The statistical analysis function of the built-in software of KEYENCE VHX-6000 ultra depth of field 3D microscope was used to measure the thickness of paint layers, pigment layers, priming layers and particles sizes of the pigment. The measurement results are shown in Table 1. The thickness of paint layers are various in different positions of the sample locations. The D1−2 paint layer on the face is only 205 μm, while the paint layers at the gilding are relatively thick, such as the thickness of D1−7 is 895 μm. The thickness of pigment layers and priming layers are also different, with the thinnest only 10 μm and the thickest up to 570 μm. The thickness of gilding layers (gold foil) are only about 2 μm (as determined with SEM−EDX), while the thickness of adhesive layers are about 35−70 μm. The pigment particles size of different pigment layers also varies greatly, for example, the average diameter of black pigment particles in D1−11 L1 is less than 1 μm, while the average diameter of orange pigment particles in D1−14 L3 is 35 μm. Figure 4 are the micrographs of pigment particles observed by the microscope under different light sources and the distribution maps of pigment particles were fitted by the micrograph under coaxial light source (bright field).

Tong *et al. Herit Sci*   (2021) 9:117

Page 7 of 21

Table 1 Summary of the thickness of paint layers, pigment, priming layers and particles size

Samples No	Thickness of paint layers/μm	Thickness of pigment or gilding layers layers/μm	Particles size (min/max/average diameter/μm)	Thickness of priming or adhesive layers/μm	Particles size (min/max/average diameter/μm)
D1–1	580	L1 Reddish–brown 55	3/35/7	L2 White 85	5/35/13
		L3 Red 20	3/13/6	L4 White 55	3/15/7
		L5 Orange 35	5/17/13	L6 White 55	3/27/5
		L7 Yellow 50	3/17/5	L8 Grey 105	3/15/5
		L9 Orange 60	4/17/13	L10 White 45	2/9/4
		L11 Red 20	3/14/6	L12 White 50	3/15/5
		L13 White 30	3/10/4	L14 Grey 45	6/38/15
D1–2	205	L1 Reddish–brown 110	3/35/8	L2 Gray 60	3/23/7
D1–4	380	L1 Orange 45	3/40/20	L2 White 190	7/45/17
		L3 White 105	3/12/5	L4 Gray 40	6/40/15
D1–5	560	L1 Blue 20	3/15/8	L2 Gray 95	6/33/13
		L3 White 25	2/6/4	L4 Gray 155	4/27/15
		L5 Red 10	3/7/5	L6 Gray 50	4/26/7
		L7 Green 205	8/60/18	L8 Gray 50	3/19/6
D1–6	425	L1 Red 30	2/30/7	L2 Gray 110	4/32/12
		L3 White 30	3/30/7	L4 Gray 50	3/47/10
		L5 White 20	2/6/3	L6 White 70	3/17/8
		L7 White 15	2/6/3	L8 Gray 110	5/28/10
D1–7	895	L1 Gold 2	–	L2 Brown-black 60	–
		L3 Golden yellow 35	3/45/12	L5 Black 65	–
		L4 Gold 2	–	L8 Black 65	–
		L6 Golden yellow 45	3/30/10	L10 Black 65	–
		L7 Silver 2	–	L12 Black 70	–
		L9 Silver 2	–	L13 White 75	4/27/10
		L11 Gold 2	–	L15 Black 35	–
		L14 Gold 2	–	L16 White 240	5/48/20
D1–8	350	L1 Pink 40	3/20/7	L2 White 130	14/47/25
				L3 Claybank 205	10/41/15
D1–9	370	L1 Gold 2	–	L2 Black 45	–
		L3 Golden yellow 80	4/68/13	L5 Black 10	–
		L4 Gold 2	–	L8 Black 35	–
		L6 Golden yellow 25	3/21/12	L10 Black 70	–
		L7 Gold 2	–	L12 Brown 45	–
		L9 Gold 2	–	L14 Black 45	–
		L11 Gold 1	–	L15 Gray 105	4/51/15
		L13 Gold 2	–		
D1–11	210	L1 Black 35	<1	L2 Gray 25	3/12/8
		L3 Orange 30	4/27/11	L4 White 35	5/26/8
D1–12	225	L1 Reddish-brown 120	4/70/13		
		L2 Black 70	<1		
D1–13	250	L1 Red 30	4/35/8	L5 Claybank 60	7/23/10
		L2 Orange 25	3/20/6	L6 Gray 50	12/35/15
		L3 Red 35	3/12/6		
		L4 White 30	3/15/6		
D1–14	345	L1 Yellow 70	4/30/17		
		L2 Green 65	13/61/23		
		L3 Orange 130	14/110/35		
		L4 Green 45	14/52/22		

Tong *et al. Herit Sci*   (2021) 9:117

Page 8 of 21

Table 1 (continued)

Samples No	Thickness of paint layers/μm	Thickness of pigment or gilding layers layers/μm	Particles size (min/max/average diameter/μm)	Thickness of priming or adhesive layers/μm	Particles size (min/max/average diameter/μm)
D1–15	745	L1 Green 570	12/68/25	L4 White 60	3/15/7
		L2 Black 10	<1		
		L3 Red 25	3/12/6		
		L5 Red 20	3/13/6		
D1–16	225	L1 Red 50	3/65/8	L2 White 40	3/11/5
		L4 Orange 45	5/24/10	L3 Brown 95	–
D1–17	870	L1 White 290	8/75/16	L2 White 145	5/35/10
D1–18	290	L1Blue-green 75	15/35/20	L3 Gray 35	3/17/10
		L2 Black 50	<1		
		L4 Black 90	<1		

The pigment layers and the priming layers usually appear alternatively, indicating that during repainting the statue was generally primed with a white layer that was applied over the last pigment layer. For the gilding layers very few priming layers are found. Instead new gold foil layers were applied directly over the last gold foil using an adhesive. In some places there is no priming layers between the old and new pigment layers. For example, the orange pigment layer L1 of the D1–12 was applied directly over the black pigment layer L2 (Fig. 4a).

Paint layers represented by D1–8 and D1–19 are clearly different from other paint layers in terms of layer structure. The whole paint layers were painted on a layer of white paper (Fig. 3t, x, paper fibers are attached to the back of the paint layers), and the white paper was pasted over a white ground layer. Taking D1–8 as an example, the layers from the surface to the unpainted clay is as follows: L1 pink pigment layer → L2 white priming layer → L3 brown priming layer → L4 white paper → L5 white ground layer → clay body. D1-8 and D1-19 come from the inside of the sleeves and the black cassock area and are associated with new painting technology in the latest polychromy. The application of this new painting technology was likely designed to realistically shape the texture of clothes worn by Bodhidharma statue.

Analysis of gilding layers

EDS analyses show that the gold layers of D1–7 and D1–9 contains only Au and Ag except some layers (the 11th layer of D1–7 contains 3.6% Cu). The gold content of most gold layers is more than 90%, which indicates that these gold layers are gold foils with high gold content. The thickness measured by the electron microscope is only 2 μm at the thickest point. The 7th and 9th layers of sample D1–7 can hardly be observed under the optical microscope, while they are clearly evidenced in the backscattered electron images (Fig. 3f). EDS results show that the two layers mainly contain Cl and Ag, with a mass ratio of about 1/3.7 to 1/3.2. The Raman spectrum of white particles in layer 7 (Fig. 5a) shows characteristic bands at 147vs, 221 m, 292 m cm^{-1} similar to chlorargyrite (AgCl, Fig. 5b). Combined with the results of EDS, it can be inferred that the main phase of D1–7 L7 and L9 are chlorargyrite. In terms of thickness and stratigraphic structure, D1–7 L7, L9 are only 1–2 μm in thickness like other gold foil layers. Therefore, these two layers were silver foils that were pasted on the statue surface at two separate times. Corrosion later transformed the silver foils into chlorargyrite.

The L3 and L6 of D1–7 and D1–9 paint layers appear golden yellow in cross-section with mineral granularity (Fig. 3e, i). The four layers of golden yellow material were painted over gold foil layers. From the colour and its layer position, it can be confirmed that these layers were applied over gold foils. The results of EDS show that these four layers mainly contain Al, Si, K, Ca, Fe. In addition, D1–9 L3 contains 8% Au, which is due to the curious inclusion of gold particles in this layer (Fig. 3i). The Raman spectrum of golden yellow particles in layer 3 (Fig. 5c) shows characteristic bands at 216 m, 260vs, 705 m cm^{-1} similar to pyrophyllite ($Al_2Si_4O_{10}(OH)_2$, Fig. 5d). Combined with the results of EDS, it can be inferred that the main phase of the L3 and L6 of D1–7 and D1–9 are high iron pyrophyllite clay mineral.

In ancient China, especially since the Song Dynasty (960–1279 CE), the decorative technology of embossed painting and gilding (沥粉堆金) on Buddha statues was very popular. As the saying goes, "Clothes to people, Gold to Buddha". However, the use of silver foil and gold mixed with golden yellow mineral to replace gold foil used in
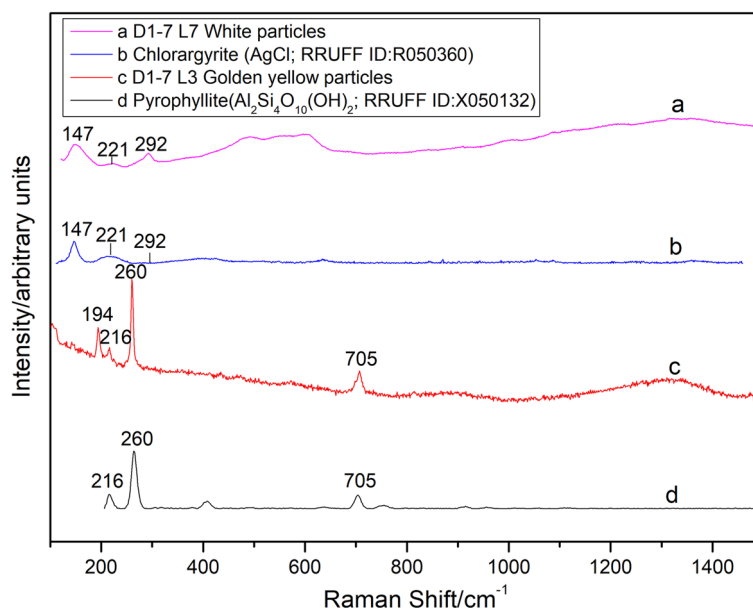
Tong *et al. Herit Sci*   (2021) 9:117

Page 9 of 21

Fig. 5 a and **c** Raman spectrum of D1–7 L7 white particles and L3 golden yellow particles, **b** and **d** Raman spectrum of chlorargyrite and pyrophyllite from the RRUFF open source database
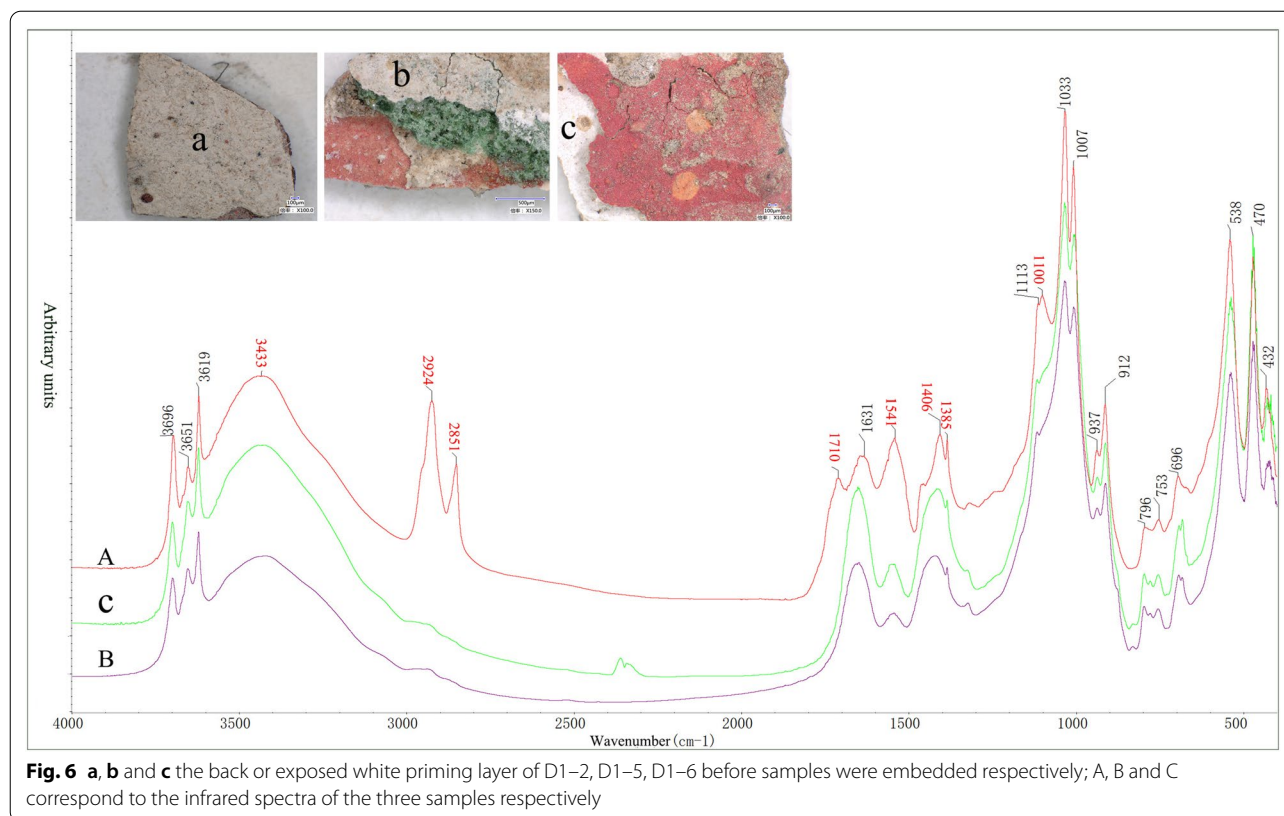
the decorating Buddha statues is rarely mentioned in the literature. The decorative technology of paste silver foils were found in ancient murals [14, 15] and architectural paintings [16] in small amounts. Pyrophyllite as a pigment was once found in bodhisattva statue of the Ming Dynasty (1368–1644 CE) grotto 51 in Maijishan (麦积山) [17]. In addition, studies show that pyrophyllite yellow clay mineral is one of the iron-containing yellow pigments used in ancient China, in which the colour composition is iron yellow (ɑ -FeOOH) [18]. The discovery of silver foil layers and golden yellow pyrophyllite mineral with gold particles in D1–7 suggests that there were other alternatives to gold that were employed to imitate gilding.

Analysis of the priming layers

In terms of element distribution, the priming under the pigment layers can be roughly divided into five types. The first type is the white mineral dominated by Al, Si (Al/Si ratio between 1/2 and 1/1.2) and containing a small amount of K, Fe, Ca, Pb and other elements, such as D1−1 with priming layers, D1−2 L2, D1−5 L2 L4 L6, D1−6 L2 L4 L6 L8, D1−11 L5. These white minerals showed no obvious Raman scattering except quartz particles. In order to determine the mineral phase of the priming layers, three samples with simple layer structure, D1−2, D1−5, D1−6, were selected for FTIR analyses. Figure 6A, B and C are the infrared spectra of the above three samples respectively, and their main

infrared characteristic absorption bands are basically one-to-one corresponding to the infrared characteristic absorption bands of kaolin [19]. Among them, the bands at 3696, 3651 cm^{-1} corresponds to the stretching vibration of Al−OH bond outside the kaolinite octahedron structure, the band at 3620 cm^{-1} corresponds to the stretching vibration of Al−OH bond within the kaolinite structure. The absorption band at 1630 cm^{-1} is the vibration band of attached water, 1113, 1033 and the band at 1007 cm^{-1} corresponds to the stretching vibration of Si−O bond, 937 cm^{-1} corresponds to the vibration of Si−O-Al bond, 912 cm^{-1} corresponds to the bending vibration of Al-O−H. The three bands of 796, 753 and 696 cm^{-1} are attributed to the stretching vibration absorption bands of Si−O, Si−Si and Si-Al generated by associated quartz and feldspar. The band near 538, 470, 432 cm^{-1} corresponds to the bending vibration of Si−O. In addition to the characteristic bands of kaolin, there are obvious infrared characteristic bands at 2924, 2851, 1710, 1406, 1385 and 1100 cm^{-1} in the infrared spectrum of D1-2 sample. These characteristic bands could be related to the organic layer of the sample L0.

The second type of priming layer mineral dominated by Al and Si (Al/Si ratio between 1/2 and 1/1.2) and containing Pb, including D1−4 L2, D1−11 L2, D1−13 L4, L5 and L6, which contain 30%-45% Pb. Lead white ($2PbCO_3 \cdot Pb(OH)_2$) particles were identified with Raman spectroscopy in layers D1−4 L2 and D1−13 L4. Therefore,

Tong *et al. Herit Sci*   (2021) 9:117

Page 10 of 21

Fig. 6 **a**, **b** and **c** the back or exposed white priming layer of D1–2, D1–5, D1–6 before samples were embedded respectively; A, B and C correspond to the infrared spectra of the three samples respectively

it can be inferred that these leaded priming layers are mixtures of kaolin and different proportions of lead white. The third type of priming layer mineral is dominated by Ca and Pb. For example, the contents of Ca and Pb in D1–4 L4 are 57% and 38%, while the contents of Al and Si are only 2% and 3%. Micro-Raman spectroscopy revealed two white minerals, chalk ($CaCO_3$) and lead white in D1–4 L4. Combined with the results of EDS show that the priming layer composed of chalk and lead white, mixed with a small amount of kaolin. The fourth type of priming layer mineral dominated by Pb, such as D1 D1–4 L411 L4 and D1 D1–4 L415 L4, containing Pb content in the two layers as high as 85% and 60% respectively. μ-RS confirmed that the main mineral phase in these two layers is lead white, so this type of priming is lead white with a small amount of kaolin added. The fifth type of priming layer mineral dominated by Si, Al, Ca, and containing a certain amount Fe. For example, under the pink pigment layer of D1–8 sample, there are two priming layers of white and brown, and the Al/Si ratio of their chemical composition are about 1:3. Both of these two layers contain Fe (the white layer 13% and the brown layer 16%), which is different from other kaolin-based priming layers mineral in chemical composition. The priming of these two layers have no obvious Raman activity. According to the relative content of elements, it can

be inferred that the white priming layer should be a clay with low aluminum and high calcium, while the brown priming layer is a clay with low aluminum and high iron.

In summary, the priming layers material used in each previous polychrome of the statue is mostly white kaolin or a mixture of other white minerals based on kaolin as the matrix. The use of a kind of priming material with low aluminum and high iron in D1–8 is obviously different from other paint layers.

Analysis of pigment layers

The results of μ-RS analyses of mineral pigments in each pigment layers are shown in Table 2. Raman analyses are based on published literature [20, 21]. Raman spectra of some pigments are shown in Figs. 8 and 9. Table 3 shows the L*a*b* values of different colors at each sampling position on the statue surface measured by the X-Rite VS450 non-contact spectrophotometer.

Reddish–brown pigment layers

The reddish–brown pigment layers have three layers: D1–1 L1, D1–2 L1 and D1–12 L1. μ-RS analyses show that the D1–1 L1 and D1–2 L1 pigment layers are composed of hematite (Fe_2O_3) and red lead (Pb_3O_4). EDS analyses show that the Fe content in the two layers are significantly different (17%, 31%, respectively), indicating

Tong *et al. Herit Sci* (2021) 9:117

Page 11 of 21

Table 2 Results of SEM–EDS and μ-RS analyses

Samples No	Layers No	Al (Cr)	Si	K (Na)	Ca (Mg)	Fe (Ti)	Pb (Au)	As (Ag)	S (Cl)	Hg (Cu)	μ-RS results
D1-1	L1 Reddish- brown	3.6	12.1	1.5	4.6 (0.9)	17.5	59.8	–	–	–	Hematite, red lead
	L2 Priming layer	23.6	37.3	3.7	8.7	4.4	20.0	2.3	–	–	–
	L3 Red	0.7	0.9	–	–	–	–	–	14.9	83.5	Cinnabar
	L4 Priming layer	18.8	35.5	3.9	17.6	7.0	17.2	–	–	–	–
	L5 Orange	3.8	2.6	–	2.5	–	81.6	9.5	–	–	Red lead
	L6 Priming layer	33.0	42.6	3.3	–	3.1	14.2	3.7	–	–	–
	L7 Yellow	4.1	5.0	–	–	–	22.8	44.6	23.4	–	Orpiment
	L8 Priming layer	29.8	35.2	–	6.8	3.8	16.1	8.3	–	–	–
	L9 Orange	3.6	3.8	–	2.4	–	90.3	–	–	–	Red lead
	L10 Priming layer	18.5	32.6	3.3	18.3	5.8	21.3	–	–	–	–
	L11 Red	–	–	–	–	–	15.4	–	11.5	73.1	Cinnabar
	L12 Priming layer	24.2	49.5	4.0	1.8	2.5	17.9	–	–	–	–
	L13 White	–	3.7	–	12.9 (3.5)	–	79.9	–	–	–	Lead white, chalk
D1–2	L1 Reddish– brown	–	8.4	–	1.6	26.4	63.6	–	–	–	Hematite, red lead
	L2 Priming layer	39.1	49.5	1.8	2.9	6.7	–	–	–	–	–
D1-3	L1 Pink	25.3	45.1	4.3	8.1 (2.4)	13.5 (1.3)	–	–	–	–	Hematite, Anatase titanium white
D1–4	L1 Orange	2.9	3.2	1.0	1.2	–	91.7	–	–	–	Red lead
	L2 Priming layer	22.9	25.2	2.2	2.8	–	46.9	–	–	–	Lead white,
	L3 White	1.4	1.8	–	11.9	–	84.9	–	–	–	Lead white, chalk
	L4 Priming layer	1.5	3.3	–	56.5	–	38.7	–	–	–	Chalk, lead white,
D1–5	L1 Blue	13.8	23.6	(1.5)	43.8	4.0	10.5			(2.7)	Azurite, chalk
	L2 Priming layer	37.3	52.5	5.4	–	4.8	–	–	–	–	–
	L3 White	0.6	0.7	–	–	–	98.7	–	–	–	Lead white
	L4 Priming layer	27.1	53.3	7.4	3.0	2.7	6.5	–	–	–	–
	L5 Red	6.5	6.8	3.5	9.8 (3.9)	–	33.8	–	9.1	26.7	Cinnabar, red lead
	L6 Priming layer	31.1	51.6	8.6	4.5	4.2	–	–	–	–	
	L7 Green	4.1	22.4	–	29.1 (12.1)	–	–	–	–	(32.4)	
	L8 Priming layer	18.5	23.6	2.8	52.0	3.1	–	–	–		
D1-6	L1 Red	-	-	–	1.7	–	–	–	21.3	77.0	Cinnabar
	L2 Priming layer	30.7	50.3	8.4	10.6	–	–	–	–	–	
	L3 White	–	4.6	–	29.2 (13.6)	–	52.6	–	–	–	Chalk, magnesite, lead white
	L4 Priming layer	38.0	51.9	6.6	3.6	–	–	–	–	–	
	L5 White	0.8	–	–	1.3	-	97.9	-	–	–	Lead white
	L6 Priming layer	27.7	59.2	8.3	1.8	3.0	-	-	–	–	
	L7 White	1.4	0.9	–	1.0	-	96.7	-	–	–	Lead white
	L8 Priming layer	37.9	50.5	5.9	–	5.7	-	-	–	–	
D1-7	L1 Gold	–	–	–	–	–	(89.1)	(10.9)		–	
	L3 Golden yellow	23.6	43.1	5.7	4.0	23.6	–	–	–	–	Pyrophyllite
	L4 Gold	–	–	–	–	–	(93.1)	(6.9)		–	
	L6 Golden yellow	27.1	37.1	5.5	3.2	25.3				(1.8)	
	L7 Silver	–	–	–	–	–	–	(78.6)	(21.4)		
	L9 Silver	–	–	–	–	–	–	(73.6)	(23.0)	(3.4)	
	L11 Gold	–	–	–	–	–	(89.1)	(7.3)		(3.6)	
D1-8	L1 Pink	8.5	24.0	–	37.1 (8.4)	19.0	-	-	3.0	–	Hematite, chalk
	L2 Priming layer	12.8	42.0	5.5	26.7	13.0	-	-	-	–	
	L3 Priming layer	16.5	49.1	7.9	10.3	16.2	-	-	-	–	

Tong *et al. Herit Sci*   (2021) 9:117

Page 12 of 21

Table 2 (continued)

Samples No	Layers No	Al (Cr)	Si	K (Na)	Ca (Mg)	Fe (Ti)	Pb (Au)	As (Ag)	S (Cl)	Hg (Cu)	μ-RS results
D1-9	L1 Gold	–	–	–	–	–	(97.4)	(2.6)		–	
	L3 Golden yellow	18.9	45.6	4.2	3.6	19.5	(8.2)	–		–	
	L4 Gold	–	–	–	–	–	(96.7)	(3.3)		–	
	L6 Golden yellow	28.8	38.2	5.8	5.2	22.0	–	–	–	–	
	L7 Gold	–	–	–	–	–	(96.6)	5.4		–	
	L13 Gold	–	–	–	–	–	(90.2)	9.8		–	
D1–10	L1 Blue	19.9	34.1	2.8 (19.4)	1.1	–	–	–	21.1 (1.6)	–	Ultramarine
D1–11	L1 Black										Lamp black
	L2 Priming layer	27.7	32.8	–	9.2	(0.5)	29.8	–	–	–	
	L3 Orange	1.9	1.5	–	1.4	–	88.4	–	(6.8)	–	Red lead
	L4 Priming layer	3.3	3.6	–	–	–	83.4	–	(9.7)	–	Lead white
	L5 Priming layer	28.1	48.3	3.9	–	(0.7)	19.1	–	–	–	
D1–12	L1 Reddish– brown	0.5	–	–	0.4	–	95.4	–	(3.7)	–	Red lead
	L2 Black										Lamp black
	L3 Priming layer	10.9	23.0	–	16.2 (8.5)	–	41.4	–	–	–	
D1–13	L1 Red	1.8	2.9	–	9.6	–	–	–	19.8	65.9	Cinnabar
	L2 Orange	0.7	0.8	–	–	–	98.5	–			Red lead
	L3 Red	2.9	4.0	–	3.6	–	–	–	8.2	81.3	Cinnabar
	L4 White	25.6	33.7	3.2	3.0	–	34.5	–	–	–	Lead white
	L5 Priming layer	18.1	35.4	5.0	(2.1)	5.8	33.6	–	–	–	
	L6 Priming layer	18.9	28.0	3.0	8.9	–	39.2	–	–	–	
D1–14	L1 Yellow	(0.5)	1.4	–	30.3	–	60.4	7.4	–	–	Chrome yellow, chalk
	L2 Green	1.6	5.3	–	3.9	–	48.3	26.0	(3.0)	(11.9)	Emerald green
	L3 Orange	0.7	0.9	–	–	–	98.4	–	–	–	Red lead
	L4 Green	2.2	2.3		2.6	–	74.8	9.9	(2.1)	(6.1)	Emerald green
D1–15	L1 Green	–	6.1	–	4.2	–	–	58.9	–	(30.8)	Emerald green
	L2 Black										Lamp black
	L3 Red	–	5.0	–	4.2	–	–	4.2	36.2	50.4	Cinnabar
	L4 Priming layer	10.7	21.2	–	–	–	59.7	8.4	–	–	
	L5 Red	1.0	1.4	–	3.1	–	48.9	7.1	12.7	25.8	Cinnabar
D1–16	L1 Rose red										Rhodamine B
	L2 White	2.3	4.7	–	20.6	(54.6)	–	–	17.8	–	Anatase titanium white
	L4 Orange	6.1	12.6	–	11.9 (6.9)	59.7	–	–	2.8	–	Hematite
D1–17	L1 White	8.0	16.4	1.9	70.8 (2.9)	–	–	–	–	–	Chalk
D1–18	L1 Blue–green			(3.6)	4.8		53.3	(0.4)	(37.9)		Lavendulan
	L2 Black										Lamp black
D1–19	L1 Black										Lamp black

that the different colour requirements of the pigment layers at different locations (D1–2 L1 is darker in colour than D1–1 L1). The pedestal area represented by D1–12 L1 is reddish-brown (Fig. 2), while the pigment layer presents a bright orange–red on the cross-section (Fig. 4a).

Raman analysis shows that the orange-red mineral is red lead (Pb_3O_4). The change from bright orange–red to reddish–brown on the exposed surface of the pigment layer should be related to the oxidation and deterioration of red lead pigments, and it is well known that red lead can

Tong *et al. Herit Sci*   (2021) 9:117

Page 13 of 21

Table 3 The L* a * b * values of various colour on the surface of the Dharma statue

Samples No	Measuring position	Colour	L*	a*	b*
D1–2	Right side of the face	Reddish–brown	30.9	9.5	8.1
D1–4	Collar	Orange	52.8	15.5	16.6
D1–6	Collar	Red	42.7	36.3	23.2
D1–7	Collar embossed painting and gilding	Golden	58.8	4.7	23.6
D1–8	Inside the right cuff	Pink	54.5	12.8	12.0
D1–9	Chest	Golden	42.7	12.0	28.4
D1–10	The pattern on the chest	Blue	32.3	− 0.9	− 17.4
D1–11	Near edge of pedestal	Black	20.1	− 0.1	0.7
D1–12	Pedestal	Reddish–brown	32.0	15.3	12.4
D1–13	The right sleeve	Red	33.1	27.8	16.9
D1–14	The yellow flower on the right sleeve	Yellow	66.8	7.5	36.5
D1–15	The left sleeve	Green	34.5	− 11.2	14.1
D1–16	The bottom step area of the pedestal	Rose	51.9	27.8	11.0
D1–17	The pattern on the chest	White	65.3	2.2	11.5
D1–18	The pattern on the surface of cassock	Blue–green	44.1	− 9.1	8.6
D1–19	Cassock	Black	23.0	− 0.4	1.5

be transformed into brown-black lead dioxide (PbO_2) in high humidity environment [22–24].

Red pigment layers

There are eight red pigment layers: D1–1 L3, L11, D1–5 L5, D1–6 L1, D1–13 L1, L3, D1–15 L3, L5. Raman analyses show that the mineral composition of the red pigment layers are mainly cinnabar (HgS) except for D1–5 L5. EDS analyses results also show that these pigment layers mainly contain Hg and S except for a small amount of Si, Al, Ca and other elements. D1-5 L5 is made of two minerals, cinnabar and red lead.

Orange pigment layers

There are seven orange pigment layers: D1–1 L5, L9, D1–4 L1, D1–11 L3, D1–13 L2, D1–14 L3 and D1–16 L4. μ-RS analyses show that the mineral phase of D1–16 L4 is hematite (Fe_2O_3), and the rest of the pigment layers are all red lead (Pb_3O_4). EDS analyses results show that the content of Pb in the pigment layers containing red lead are above 90%, which indicates that these pigment layers are basically composed of pure red lead.

Pink pigment layers

The pink pigment layers are D1–3 L1 and D1–8 L1. D1–3 L1 is composed of hematite (Fe_2O_3) and anatase titanium dioxide (TiO_2), while D1–8 L1 is composed of hematite and chalk ($CaCO_3$) (the relative mass ratio of Ca(Mg) to Fe element is 2.4/1). The pink paint layer D1–3 L1 is directly painted on the unpainted clay idol (Fig. 3u). This is obviously different from the characteristics of paint layer painted over white paper in D1–8 L1, so it can be

inferred that the pink area of hematite + anatase titanium dioxide in D1–3 L1 is a repair place after partial damage and shedding of the original hematite + chalk pink area.

Blue pigment layers

The blue pigment layers are D1–5 L1 and D1–10 L1. Raman analyses shows that the blue mineral in D1–5 L1 is azurite ($Cu_3(CO_3)_2(OH)_2$), and there are white chalk ($CaCO_3$) particles mixed in L1. D1–10 L1 mineral Raman characteristic bands at 258w, 548vs, 1091 m cm^{-1} (Fig. 8j) are completely consistent with the characteristic bands of ultramarine. Raman spectrum and chemical composition cannot distinguish natural and synthetic ultramarine pigment, but polarizing microscope analysis is an effective and simple method. Natural ultramarine pigment is made of lapis lazuli mineral grinding, because lapis lazuli mineral is often accompanied by diopside, calcite, pyrite, so there are more impurities in the pigment; particles shape are irregular, angular, with particles diameter in the 10–20 μm interval. But artificial ultramarine pigment is pure in texture, and the particles shape are regular, uniform and fine (average diameter is 5 μm) [25]. D1–10 L1 blue pigment is bright and colourful under plane polarized light (Fig. 7a), with pure texture, smooth particle edge, particles diameter are 3–6 μm, completely extinction under orthogonal polarized light (Fig. 7b), which correspond to the characteristics of artificial ultramarine pigment ($Na_{6-10}Al_6Si_6O_{24} S_{2-4}$).

Yellow pigment layers

There are six yellow pigment layers: D1–1 L7, D1–14 L1, D1–7 L3, L6, D1–9 L3, L6. As discussed in the "Analysis

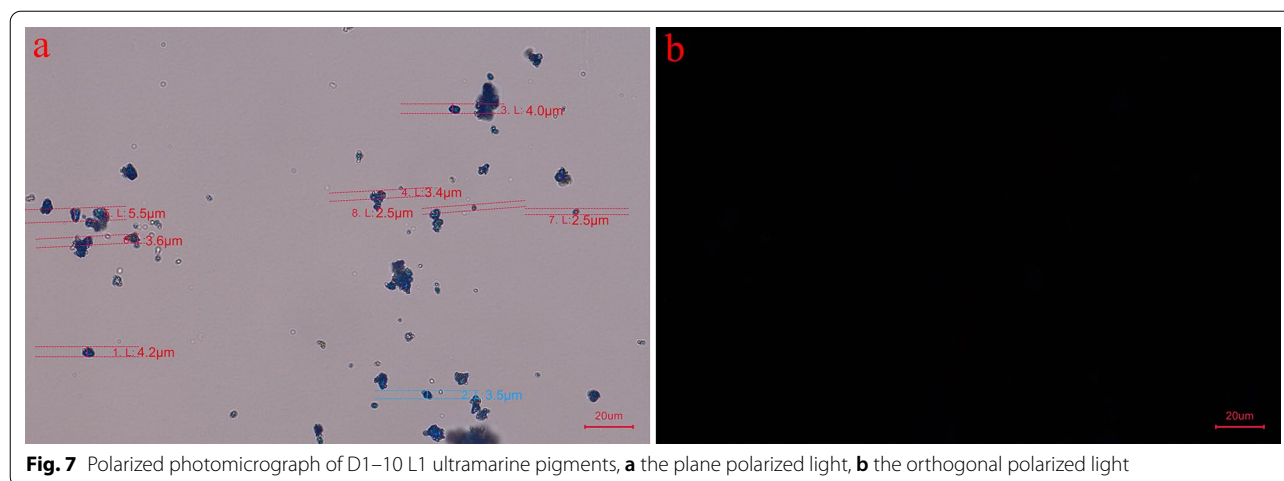Tong *et al. Herit Sci*   (2021) 9:117

Page 14 of 21

Fig. 7 Polarized photomicrograph of D1−10 L1 ultramarine pigments, **a** the plane polarized light, **b** the orthogonal polarized light

of gilding layers" section, the golden minerals in D1−7 and D1−9 L3, L6 were high iron pyrophyllite clay minerals that were used to replace gold foil. D1−1 L7 mainly contains As, S, Pb, and Raman analysis shows that the main mineral phase is orpiment (As_2S_3). In cross-sections of D1−14 L1 (Fig. 9d), it can be clearly seen that yellow mineral particles and white mineral particles are mixed together. According to Raman analyses, yellow pigment particles are chrome yellow ($PbCrO_4$, Fig. 9e), and white pigment particles are chalk ($CaCO_3$). Chrome yellow is a synthetic pigment that appeared in the early nineteenth century [26]. There are three types of chrome yellow pigments used by artists. Depending on the sulfate amount, chrome yellow is nowadays named Primrose Chrome ($PbCr_{1-x}S_xO_4$, $0.4 \leq x \leq 0.5$), Lemon Chrome ($PbCr_{1-x}S_xO_4$, $0.2 \leq x \leq 0.4$) and Middle Chrome (mainly pure $PbCrO_4$) [27]. The studies show that [27, 28] the S-rich chromium yellow pigment has obvious Raman signal of the $v_1(SO_4^{2-})$ mode at near 973 cm^{-1}. In the D1−14 L1 chrome yellow Raman spectrum, the $v_1(CrO_4^{2-})$ mode at 841 cm^{-1}, and the five modes in the Cr−O bending region at 401, 377, 359, 337, 325 cm^{-1}, no $v_1(SO_4^{2-})$ mode could be detected. These results indicate that the chromium yellow in D1−14 L1 should be Middle chromium yellow, that is, pure lead chromate ($PbCrO_4$).

White pigment layers

There are seven white pigment layers: D1−1 L13, D1−4 L3, D1−5 L3, D1−6 L3, L5, L7, D1−17 L1. The Ca element in D1−17 L1 is as high as 70.8%, and Raman analysis shows that the main mineral is chalk ($CaCO_3$). D1−6 L3 mainly contains Pb, Ca and Mg. Raman analyses shows that the main mineral phase in this layer are lead white ($2PbCO_3 \cdot Pb(OH)_2$), chalk,

and magnesite ($MgCO_3$). Both D1−1 L13 and D1−4 L3 mainly contain Pb, Ca, and the relative contents of the two elements are about 80% and 12%. Combined with Raman analyses, these two layers are lead white and chalk. The relative content of Pb in the other white pigment layers (D1−5 L3, D1−6 L5, L7) are as high as 96%, and Raman analyses shows that the main mineral phase is lead white.

Green pigment layers

There are five green pigment layers: D1−5 L7, D1−14 L2, D1−14 L4, D1−15 L1, D1−18 L1. D1−5 L7 mainly contains Cu, Ca, Mg and Si, among which Cu content is the highest (32%). The green pigment layer shows no obvious Raman activity. Because the pigment layer appears glassy under microscope (Fig. 8c), it is likely that the layer is a copper-containing pigment in a glassy state. D1−14 L2, L4 and D1−15 L1 mainly contain Cu and As, with characteristic Raman bands at 122w, 154vs, 175vs, 217vs, 242vs, 294 m, 325 m, 371 m, 429 m, 492 m, 539 m, 637vs, 685w, 760w, 835w, 951 m cm^{-1} (Fig. 9f) corresponding to bands emerald green pigment ($Cu(C_2H_3O_2)2 \cdot 3Cu(AsO_2)_2$). D1−18 L1 minerals are blue−green in colour and contain As, Cu, Ca, Na and Cl. The Raman spectrum (Fig. 9h) shows bands at 178w, 544 m and 856vs cm^{-1}, and is identified as Lavendulan (RRUFF ID: R141212).
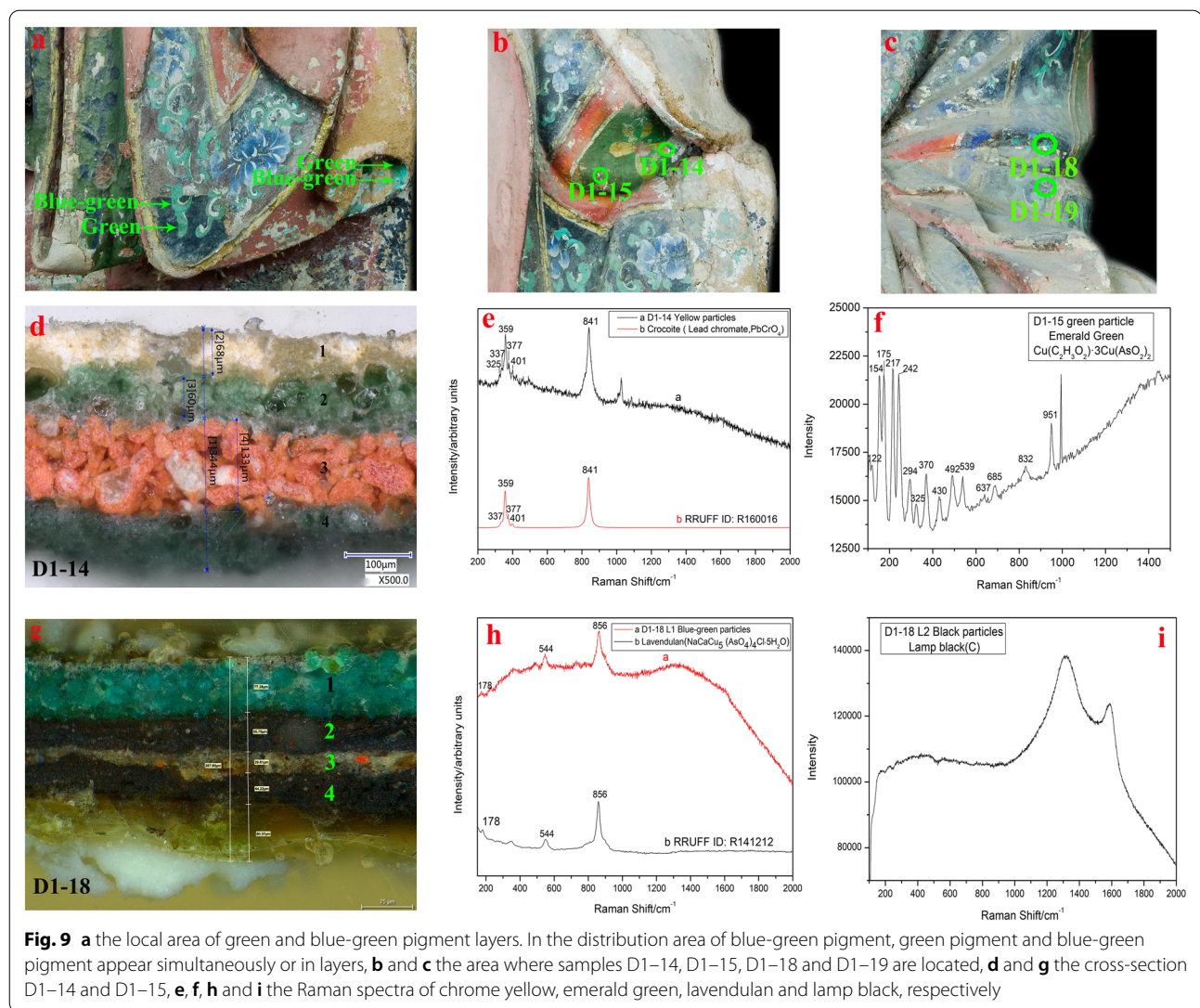
Lavendulan ($NaCaCu_5(AsO_4)_4Cl \cdot 5H_2O$) is a rare supergene arsenate mineral in oxidation zones of Cu- and As-bearing ore bodies [29]. It was first described by Breithaupt in 1837 and named as a mineral containing As, Co, Ni; Vogl describes it as blue coating from Jáchymov; Foshag published a detailed description of lavendulan and gave its refractive index [30]. Guillemin first used

Fig. 8 **a**, **c**, **e**, **g** cross-sections of D1–4, D1–5, D1–6, D1–13, respectively, and **b**, **d**, **f**, **h** are the corresponding backscattered images, **i** Raman spectrum of orpiment, hematite, red lead and cinnabar, **j** Raman spectrum of chalk, lead white, ultramarine and azurite
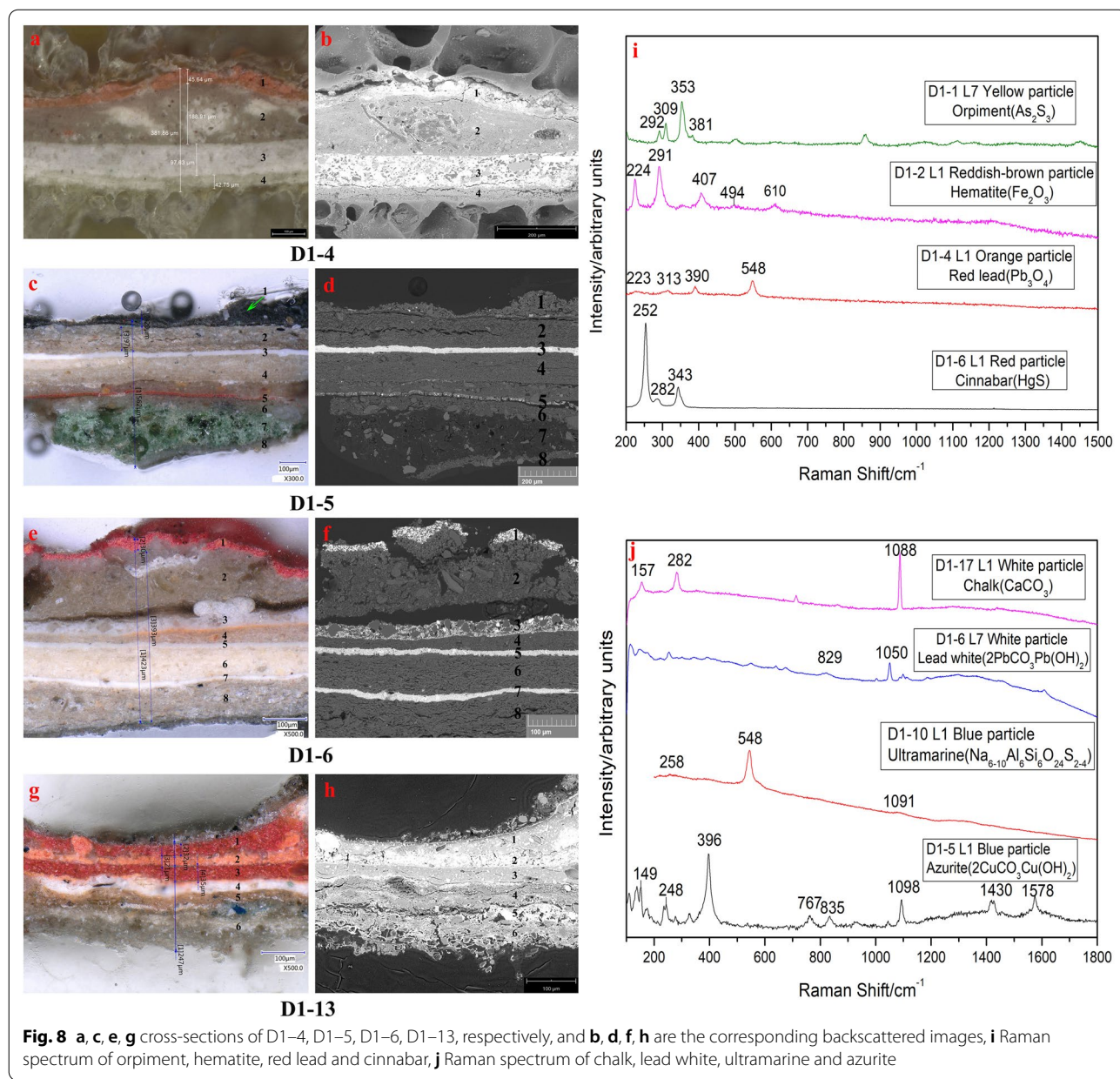
X-ray diffraction analysis to study lavendulan and proposed its original rhombic crystal structure [29]. The mineral, which has a vivid blue–green color and a small spherical or wafer-like microstructure, is often found in arid climates, and in caves derived from copper sulfides in cave walls. Also, it has been reported as an alteration products in ancient slag heaps. Further, it is certain that some of these minerals are of archaeological significance and it is apparent that they were used for cosmetics in ancient Egypt [31].

Lavendulan has also been found sporadically in Chinese polychromy such as the painted clay statue in Yungang Grottoes (云冈石窟), the coloured drawing on timber structure in Kumbum (塔尔寺) [32], the wall painting in Anyue Grottoes (安岳石窟) [33], the painted statues on Baoding Mountain in Dazu (大足宝顶山) [34–36], and the paintings of the Maidservant in the Saint Mother's Hall of Jinci Temple (晋祠) [36]. The distribution of lavendulan is extremely rare in nature. Due to its physical microscopic structure and the fact that the chemical composition is similar to the widely-used emerald green pigment from the 1830s to the early 20th century. Chinese scholars believe that the lavendulan found in polychromy is most likely an alteration product from

Tong *et al. Herit Sci* (2021) 9:117

Page 16 of 21

Fig. 9 **a** the local area of green and blue-green pigment layers. In the distribution area of blue-green pigment, green pigment and blue-green pigment appear simultaneously or in layers, **b** and **c** the area where samples D1–14, D1–15, D1–18 and D1–19 are located, **d** and **g** the cross-section D1–14 and D1–15, **e**, **f**, **h** and **i** the Raman spectra of chrome yellow, emerald green, lavendulan and lamp black, respectively

emerald green pigment, and was not intentionally used as the blue–green pigment [32–36].

In literature [36], the mechanism of corrosion conversion of emerald green pigment into lavendulan has been studied in depth. It is suggested that emerald green ($Cu(C_2H_3O_2)_2 \cdot 3Cu(AsO_2)_2$) is first dissociated into copper ions (Cu^{2+}) and arsenite ions ($(AsO_2)^-$) in a slightly acidic and humidity environment. The $(AsO_2)^-$ is oxidized to arsenate ion ($(AsO_4)^{3-}$), and finally Cu^{2+}, $(AsO_4)^{3-}$ reacts with soluble K^+, Ca^{2+}, Cl^- from the environment to produce lavendulan. There are no residual emerald green pigment particles were found in the blue–green pigment layer D1–18 L1. However, the simultaneous presence of layers of green and blue–green pigments can be seen in other blue–green pigment areas (Fig. 9a), which shows the signs of green emerald green transformation into

blue–green lavendulan. Therefore, it can be inferred that the blue–green pigment layer D1–18 L1 (the part of plant and flower pattern above the black pigment layer of the cassock of the Bodhidharma statue, as shown in Fig. 2) may have transformed from emerald green. The thickness of the pigment layer in D1–18 L1 is 75 μm, and its mineral phase was almost completely transformed into blue–green lavendulan, while the emerald green pigment layer D1–15 L1, with a thickness of 570 μm has no sign of alteration. This observation suggests that the transformation of emerald green pigment depends on the thickness of the pigment layer, with thinner pigment layers exhibiting lavendulan. This could be because the thinner the pigment layer, the easier it is to contact with the moisture and acid substances in the air, and also easier it is for the soluble salt ions to migrate in the pigment

Tong *et al. Herit Sci*   (2021) 9:117

Page 17 of 21

layer, accelerating the transformation of emerald green to lavendulan.

Black pigment layers

There are five black pigment layers: D1–11 L1, D1–12 L2, D1–15 L2, D1–18 L2 and D1–19 L1. The Raman spectra of the black pigments show two broad bands near 1325 cm^{-1} and 1580 cm^{-1} (Fig. 9 i), which is consistent with the standard Raman spectrum of lamp black (C).
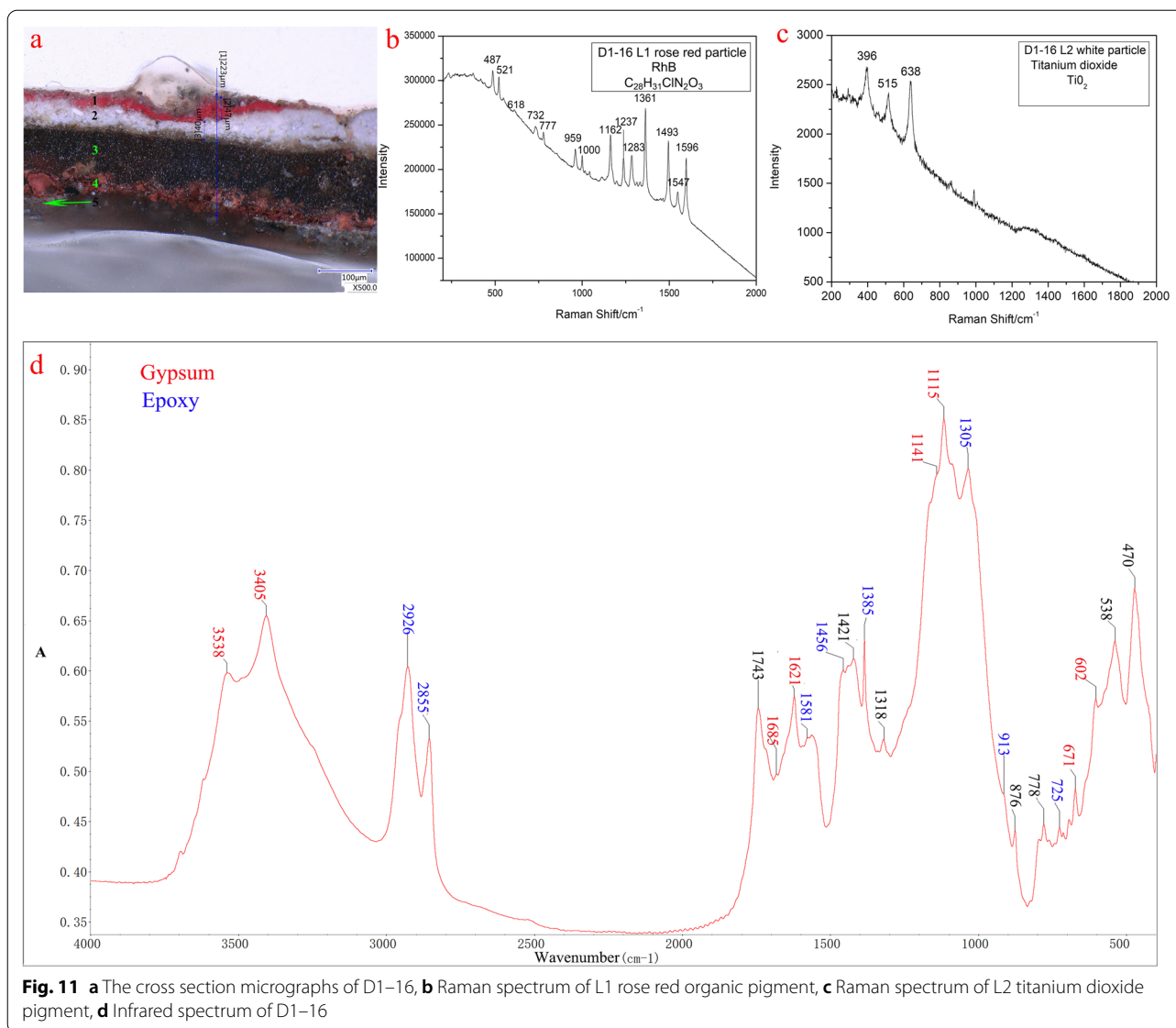
Modern rose red paint layer

The rose red paint layer is only distributed in the bottom step area of the statue pedestal represented by D1–16. From the preserved photos [37], this area was originally reddish brown before restoration and protection in 1981, and the paint layer was largely peeled off (see Fig. 10a). According to the interview with the staff of Lingyan Temple, the rose red area was painted in the restoration and protection of the Arhat statues in 1981; in addition, a layer of varnish was also painted in the bottom step area of pedestal in order to isolate moisture [1].

EDS analysis shows that the mass percentage of C and O elements in D1–16 L1 is more than 75% consistent with an organic pigment. The characteristic bands in the Raman spectrum (Fig. 11b) near 618, 732, 1000, 1233, 1283, 1361, 1493, 1547, 1595 cm^{-1} match the Rhodamine B ($C_{28}H_{31}ClN_2O_3$) [38]. The white priming layer of D1–16 L2 mainly contains Ti, Ca and S. Raman analysis confirms that the layer contains anatase titanium dioxide (TiO_2, Fig. 11c). The infrared spectrum of the D1–16 is shown in Fig. 11d, in which the absorption bands around 3538, 3405 cm^{-1} and 1685, 1621 cm^{-1} correspond to the stretching and bending vibration of water; the absorption bands around 1141, 1115 cm^{-1} correspond to the symmetric and asymmetric stretching vibration of $(SO_4)^{2-}$, and the bands around 671, 602 cm^{-1} correspond to the bending vibration of $(SO_4)^{2-}$. The characteristic bands correspond to the infrared characteristic absorption bands of gypsum ($CaSO_4 \cdot 2H_2O$) [39]. D1–16 L3 appears

Fig. 10 Comparison between the current state of the Bodhidharma Statue and the state before the conservation and restoration in 1981. **a** The state before 1981, and the picture is from literature [37], **b** the current state

Fig. 11 **a** The cross section micrographs of D1−16, **b** Raman spectrum of L1 rose red organic pigment, **c** Raman spectrum of L2 titanium dioxide pigment, **d** Infrared spectrum of D1−16

brown–black, and the content of C and O elements in this layer is more than 85%, which should be some kind of organic matter. The infrared spectrum of D1–16, in addition to the characteristic absorption bands of gypsum, exhibits bands in the vicinity of 2926, 2855, 1581, 1385 (Symmetrically deformed vibration of dimethyl in bisphenol A), 1456, 1305 (stretching vibration of fatty aromatic ether C-O), 913 (stretch vibration of epoxy ring C-O) cm^{-1}, etc. These bands basically match with the infrared characteristic bands of an epoxy resin [40], so it can be inferred that L3 was coated with epoxy resin on the bottom step of pedestal for moisture insulation in the previous restoration. Raman analysis shows that the orange—red mineral pigment in L4 is ochre (Fe$_2$O$_3$).

The determination of the minerals composition of the outermost pigment layers may also provide a basis for the estimation of the repainting time of the latest paint of the Bodhidharma statue. According to the results of Raman analyses, the yellow pigment layer D1–14 L1 contains chrome yellow and chalk, and the green pigment L2 is emerald green. The L1 yellow pigment layer is the floral motif painted over the green pigment layer. It can be seen from the cross–sections that there is no priming layer between the yellow pigment layer and the green pigment layer, indicating that the two layers of pigment were painted on the surface of the statue at the same time. Chrome yellow appeared in the early 19th century [26], emerald green (chemical name "copper acetoarsenit"), was first synthesized in Germany in 1814, mainly used

Tong *et al. Herit Sci* (2021) 9:117

Page 19 of 21

in the 1830s and early twentieth century [41]. The use of chrome yellow and emerald green in the outermost pigment layer confirms that the statue was repainted later than 1814. Chinese scholars' textual research on the existing inscriptions and other materials in Lingyan Temple have unanimously concluded that the last polychrome of the arhat statues of Lingyan Temple was in the thirteenth year of the reign of Tongzhi (1874CE) [2, 42] in the Qing Dynasty(1639–1912 CE). Chrome yellow and emerald green were most likely painted on the surface of the statue in the 1874 redecoration. The use of anatase titanium dioxide pigment in D1–3 pink pigment layer and D1–16 L2 indicated that the statue had also been treated after 1874, because the commercial titanium dioxide pigment appeared in 1916 [43]. There is no mention of the polychrome repainting of the arhat statues in Lingyan Temple after 1874 in various Chinese documents. From the photographs taken before the restoration of the Bodhidharma statue in 1981 (Fig. 10a), it can be seen that the state of the pink area from D1–3 (the inside of the hat) before 1981 is similar to its current condition. Based on the use time of anatase titanium dioxide, it can be inferred that the pink area containing anatase titanium dioxide should has been painted between 1920s to the 1980s. In addition, the Bodhidharma statue was painted with a rose red organic pigment on the previously reddish–brown step area. In summary, the most recent large–scale repainting of the statue took place in 1874, and there have been at least two partial repainting treatments since then.

Conclusions

Based on the scientific analyses of the painted layers of Lingyan Temple's Bodhidharma statue, there are some insights.

The statue has been painted at least eight times and there have been at least two partial repainting treatments in the 20th C. Before each new polychrome, white wash was applied over the last pigment layer. In the most recent polychrome, a new technique of pasting white paper on the clay figure surface and then painting the priming layer and the pigment layer was used in some areas.

The gold layer in the gilding decoration area mostly uses gold foil with a high content of gold, and its thickness is only 1–2 μm. In different periods of history, silver foil and gold particles mixed with golden yellow mineral pigments were used to replace the original gold foil layers in the gilding area. The priming layers material used in the each previous polychrome of the statue was mostly white kaolin or a mixture of other white minerals based on kaolin as the matrix. Sometimes lead white, chalk or a minerals mixture of the two white pigments were used

as the priming layers material. In addition, the clay with a low aluminum and high iron content has been used as priming layers material in the most recent repainting.

The pigment layers of the statue were mostly composed of a single inorganic mineral, and the individual pigment layers were made of 2–3 kinds of minerals to achieve different colours. The red series mineral pigments used in the statue are cinnabar (HgS), hematite (Fe_2O_3) and red lead (Pb_3O_4); Yellow pigments include orpiment (As_2S_3) and chrome yellow ($PbCrO_4$); White pigments include lead white ($2PbCO_3 \cdot Pb(OH)_2$), chalk ($CaCO_3$) and magnesite ($MgCO_3$); Blue pigments include azurite ($Cu_3(CO_3)_2(OH)_2$) and artificial ultramarine ($Na_{6-10}Al_6Si_6O_{24}S_{2-4}$); Green pigments include 19th C. emerald green ($Cu (C_2H_3O_2)_2 \cdot 3Cu (AsO_2)_2$) and copper-containing pigments in a glassy state; Black pigments were only lamp black (C). In addition, organic pigments and anatase titanium dioxide (TiO_2) have been used in partial repainting more recently. The blue–green lavendulan mineral on the surface of the statue is not intended to be used as a blue–green pigment, but rather is a degradation product of emerald green pigment. The transformation of emerald green pigment seems related to the thickness of the pigment layer. The thinner the pigment layer, the easier it is to transform.

Based on the scientific analyses, a new understanding of the structure, material, technology and other aspects of the painted layers of Bodhidharma statue were formed. There are still open questions related to the identity of the green copper-containing pigments in glassy state. What kind of technology and materials were used in ancient China to make this kind of pigment? In addition, the determination of organic materials such as the oily substance covering the face and neck of Bodhidharma statue, the adhesive materials used to apply the gold foil in the gilding paint layers, and the pigment binder are also crucial for our original intention. Further research is needed to identify binders, and also identify the source of the chloride ions which have led to the degradation of silver and arsenic based pigments.

Tong *et al. Herit Sci*   (2021) 9:117

Page 20 of 21

Declarations

Competing interests
The authors declare that they have no competing interests.

Author details
[1]Institute of Cultural Heritage and History of Science & Technology, University of Science and Technology Beijing, Beijing 100083, China. [2]Shandong Cultural Relic Conservation and Restoration Center, Jinan 250014, Shandong Province, China. [3]International Joint Research Laboratory of Environmental and Social Archaeology, Shandong University, Qingdao 266237, Shandong, China. [4]Courtauld Institute of Art, Somerset House, Strand, London WC2R 0RN, UK.

References
1. Hu JG. Coloured sculpture restoration in Lingyan Temple in Changqing Shangdong. Archaeology. 1983;11:1025–38.
2. Zhou FS. Date of manufacture and related issues about Arhat sculpture in Lingyan Temple in Changqing, Shangdong. Cultural Relics. 1984;3:76–82. https://doi.org/10.13619/j.cnki.cn11-1532/k.1984.03.016.
3. Wang CC, Li ZhM, Wang XN, Ma QL. Scientific study of the Song Dynasty polychrome Arhat statues from the Magic Cliff Monastery in Jinan. Sci Conserv Archaeol. 2018;30(06):37–47. https://doi.org/10.16334/j.cnki.cn31-1652/k.2018.06.006.
4. Lang PL, Keefer CD, Juenemann JC, Tran KV, Peters SM, Huth NM, Joyaux AG. The infrared microspectroscopic and energy dispersive X-ray analysis of paints removed from a painted, medieval sculpture of Saint Wolfgang. Microchem J. 2003;74(1):33–46. https://doi.org/10.1016/S0026-265X(02)00101-7.
5. Franquelo ML, Duran A, Castaing J, Arquillo D, Perez-Rodriguez JL. XRF, μ-XRD and μ-spectroscopic techniques for revealing the composition and structure of paint layers on polychrome sculptures after multiple restorations. Talanta. 2012;89(1):462–9. https://doi.org/10.1016/j.talanta.2011.12.063.
6. Egel E, Simon S. Investigation of the painting materials in Zhongshan Grottoes (Shaanxi, China). Herit Sci. 2013;1:29. https://doi.org/10.1186/2050-7445-1-29.
7. Wang N, He L, Egel E, Simon S, Rong B. Complementary analytical methods in identifying gilding and painting techniques of ancient clay-based polychromic sculptures. Microchem J. 2014;114(5):125–40. https://doi.org/10.1016/j.microc.2013.12.011.
8. Hu KJ, Bai ChB, Ma LY, Bai K, Liu DB, Fan BB. A study on the painting techniques and materials of the murals in the five Northern Provinces'Assembly Hall, Ziyang, China. Herit Sci. 2013;1:18. https://doi.org/10.1186/2050-7445-1-18.
9. Mahmoud HHM. Investigations by Raman microscopy, ESEM and FTIR-ATR of wall paintings from Qasr el-Ghuieta temple, Kharga Oasis, Egypt. Herit Sci. 2014;2:18. https://doi.org/10.1186/s40494-014-0018-x.
10. Li ZM, Wang LL, Ma QL, Mei JJ. A scientific study of the pigments in the wall paintings at Jokhang Monastery in Lhasa, Tibet, China. Herit Sci. 2014;2:21. https://doi.org/10.1186/s40494-014-0021-2.
11. Fiorillo F, Fiorentino S, Montanari M, Monaco CR, Bianco AD, Vandini M. Learning from the past, intervening in the present: the role of conservation science in the challenging restoration of the wall painting marriage at Cana by Luca Longhi (Ravenna, Italy). Herit Sci. 2020;8:10. https://doi.org/10.1186/s40494-020-0354-y.
12. Wei SY, Ma QL, Schreiner M. Scientific investigation of the paint and adhesive materials used in the Western Han dynasty polychromy terracotta army, Qingzhou, China. J Archaeol Sci. 2012;39(5):1628–33. https://doi.org/10.1016/j.jas.2012.01.011.
13. Rosado L, Pevenage JV, Vandenabeele P, Candeias A, Tavares D, Lopes MdC, Alfenim R, Schiavon N, Mirão J. Multi-analytical study of ceramic pigments application in the study of Iron Age decorated pottery from SW Iberia. Measurement. 2018;118(3):262–74. https://doi.org/10.1016/j.measurement.2017.05.016.
14. Wang ZX. A study of the style of Kizil wall paintings based on their colouring, portraiture, outlining and lay out. J Xinjing Norm Univ. 2006;27(2):37–41. https://doi.org/10.14100/j.cnki.65-1039/g4.2006.02.007.
15. Zhang YJ, Zhang KN. On the booming of embossed painting and gilding craft in temple murals of song and jin dynasties in Shanxi. Shanxi Arch. 2012;6:19–21. https://doi.org/10.3969/j.issn.1005-9652.2012.06.004.
16. Liu MY. Research on Pigments for Decorative Polychrome Painting in Official Handicraft Regulations and Precedents of Qing Dynasty. Tsinghua Univ. 2019. https://doi.org/10.27266/d.cnki.gqhau.2019.000535.
17. Zhou GX. Ancient pigments in China (I). Paint and Coatings Industry. (04):43–48+5. 1990. http://www.cnki.com.cn/Article/CJFDTotal-TLGY199004012.htm.
18. Zhou GX. Ancient pigments in China (II). Paint and Coatings Industry. (01):30–36+4. 1991. http://www.cnki.com.cn/Article/CJFDTotal-TLGY199101008.htm.
19. Li XH, Jiang XP, Chen C, Tu N. Research on diffuse reflectance infrared fourier transform spectroscopy of kinds of Kaolin in various areas. Spectrosc Spect Anal. 2011;31(01):114–8. https://doi.org/10.3964/j.issn.1000-0593(2011)01-0114-05.
20. Bell IM, Clark RJH, Gibbs PJ. Raman spectroscopic library of natural and synthetic pigments (pre- ≈ 1850 AD). Spectrochim Acta Part A Mol Biomol Spectrosc. 1997;53(12):2159–79. https://doi.org/10.1016/S1386-1425(97)00140-6.
21. Burgio L, Clark RJH. Library of FT-Raman spectra of pigments, minerals, pigment media and varnishes, and supplement to existing library of Raman spectra of pigments with visible excitation. Spectrochim Acta A. 2001;57(7):1491–521. https://doi.org/10.1016/S1386-1425(00)00495-9.
22. Li ZX, Fan ZX, Sheng FL. New developments in the research of colour changes in red lead vermilion and hematite. Dunhuang Res. 1992. https://doi.org/10.13584/j.cnki.issn1000-4106.1992.01.013.
23. Li ZX. A study on the red pigments used in the mogao frescoes and mechanism of their discolouration. Dunhuang Res. 1992. https://doi.org/10.13584/j.cnki.issn1000-4106.1992.03.014.
24. Ma QL, Hu ZhD, Li ZX. Corrosion and harm of microorganisms to Frescoes pigment. Dunhuang Res. 1996;3:136–44. https://doi.org/10.13584/j.cnki.issn1000-4106.1996.03.014.
25. Aceto M, Gatti G, Agostino A, Fenoglio G, Giordano V, et al. The mural paintings of Ala di Stura (Piedmont, Italy): a hidden treasure investigated. J Raman Spectrosc. 2012;43(11):1754–60. https://doi.org/10.1002/jrs.4066.
26. Otero V, Pinto JV, Carlyle L, Vilarigues M, Cotte M, Melo MJ. Nineteenth century chrome yellow and chrome deep from Winsor and Newton™. Stud Conserv. 2017;62(3):123–49. https://doi.org/10.1080/00393630.2015.1131478.
27. Geldof M, van der Werf ID, Haswell R. The examination of Van Gogh's chrome yellow pigments in'Field with Irises near Arles' using quantitative SEM–WDX. Herit Sci. 2019;7:100. https://doi.org/10.1186/s40494-019-0341-3.
28. Monico L, Janssens K, Hendriks E, Brunetti BG, Miliani C. Raman study of different crystalline forms of $PbCrO_4$ and $PbCr_{1-x}S_xO_4$ solid solutions for the noninvasive identification of chrome yellows in paintings: a focus on works by Vincent van Gogh. J Raman Spectrosc. 2014;45(11–12):1034–45. https://doi.org/10.1002/jrs.4548.
29. Giester G, Kolitsch U, Leverett P, Turner P, Williams P. The crystal structures of lavendulan, sampleite, and a new polymorph of sampleite. Eur J Mineral. 2007;19(1):75–93. https://doi.org/10.1127/0935-1221/2007/0019-0075.
30. Ondrus P, Veselovsky F, Skala R, Sejkora J, Pazout R, Fryda J, Gabasova A, Vajdak J. Lemanskiite, $NaCaCu5(AsO4)4Cl(5H_2O$, a new mineral species from the Abundancia mine, Chile. Canad Mineral. 2006;44(2):523–31. https://doi.org/10.2113/gscanmin.44.2.523.

Tong *et al. Herit Sci*   (2021) 9:117

Page 21 of 21

31. Frost RL, Weier ML, Williams PA, Leverett P, Kloprogge J, Theo KJ. Raman spectroscopy of the sampleite group of minerals. J Raman Spectrosc. 2007;38(5):574–83. https://doi.org/10.1002/jrs.1702.

32. Chen XL, Yang Q. Micro-Raman spectroscopy study of three green pigments containing copper and arsenic. Sci Conserv Archaeol. 2015;27(3):84–9. https://doi.org/10.16334/j.cnki.cn31-1652/k.2015.03.015.

33. Chen EX, Zhang BJ, Zhao F. Comprehensive analysis of polychrome grotto relics: a case study of the paint layers from anyue, sichuan, china. Anal Lett. 2020;53(9):1455–71. https://doi.org/10.1080/00032719.2019.1709197.

34. Wang LQ, Ma YN, Zhang YX, Zhao X, He QJ, Guo JY, Ren HT. Pigment identification of sleeping buddha at world cultural heritage Dazu rock carvings with μ-Raman spectroscopy and related research. Spectrosc Spect Anal. 2020;40(10):3199–204. https://doi.org/10.3964/j.issn.1000-0593(2020)10-3199-06.

35. Cui Q, Zhang YX, Shui BW, Yu ZR, Fan ZX, Shan ZW, Chen XY, Su BM. Study of copper and arsenic-containing green and blue-green pigments of rock carvings at Big Buddha Bay in Dazu. Sci Conserv Archaeol. 2020;32(06):87–94. https://doi.org/10.16334/j.cnki.cn31-1652/k.20180601236.

36. Li ZM, Wang LL, Chen HL, Ma QL. Degradation of emerald green: scientifc studieson multi-polychrome Vairocana statue in Dazu rock carvings, Chongqing, China. Herit Sci. 2020;8:64. https://doi.org/10.1186/s40494-020-00410-2.

37. Zhang YH. Lingyan temple in shandong province. Jinan: Shandong people's publishing house; 1983. p. 63.

38. Ma Y, Hu W, Song XN, Wang ChK. Density functional theory study on Raman spectra of rhodamine molecules in different forms. Chin J Chem Phys. 2014;27(03):291–6. https://doi.org/10.1063/1674-0068/27/03/291-296.

39. Bao YS, Yang YY, Wang S, Bian J, Yu Y, Meng XS. Differences of material base of gypsum before and after processing drugs by IR spectroscopy and ICP–MS. Chin J Spectrosc Lab. 2012;29(05):3193–7. https://doi.org/10.3969/j.issn.1004-8138.2012.05.132.

40. Zhao J. Study on key analyticasl technology of bisphenol A epoxy resin system, Qingdao. Univ Sci Technol. 2016. https://doi.org/10.7666/d.D845598.

41. Scott DA. Copper and bronze in art corrosion, colorants, conservation[M]/ /MAQinglin, PANLu (trans). Beijing: Science Press; 2009. p. 270–3.

42. Zhang YH. Textual research on the ancient statue of lingyan temple in changqing. Cult Relics. 1959;12:1–17. https://doi.org/10.13619/j.cnki.cn11-1532/k.1959.12.022.

43. Walton RE. Titanium dioxide pigments. In: Walton RE, editor. Surface coatings. Dordrecht: Springer; 1993. p. 435–48.